RESEARCH ARTICLE

Fault geometry invariance and dislocation potential in antiplane crustal deformation: physics-informed simultaneous solutions

Tomohisa Okazaki[1*] , Kazuro Hirahara[1] and Naonori Ueda[1]

Abstract

Earthquake-induced crustal deformation provides valuable insights into the mechanisms of tectonic processes. Dislocation models offer a fundamental framework for comprehending such deformation, and two-dimensional antiplane dislocations are used to describe strike-slip faults. Previous earthquake deformation analyses observed that antiplane dislocations due to uniform fault slips are influenced predominantly by fault tips. Here, we state a general principle of fault geometry invariance in antiplane dislocations and exploit its theoretical consequence to define dislocation potentials that enable a streamlined crustal deformation analysis. To demonstrate the benefits of this theory, we present an analytical example and construct a rapid numerical solver for crustal deformation caused by variable fault slip scenarios using physics-informed neural networks, whose mesh-free property is suitable for modeling dislocation potentials. Fault geometry invariance and the dislocation potential may further the analysis of antiplane crustal deformation, particularly for uncertainty quantification and inversion analysis regarding unknown fault geometries in realistic crustal structures.

Keywords Crustal deformation, Antiplane dislocation, Fault geometry invariance, Dislocation potential, Physics-informed neural network

1 Introduction

Large earthquakes and associated processes cause substantial crustal deformation that reaches the Earth's surface, and their observation and modeling elucidate the source mechanisms and underlying physical processes (Pollitz et al. 2001; Freed and Bürgmann 2004; Sun et al. 2014). Crustal deformation has been analyzed using dislocation models that treat fault motions as displacement discontinuities in the continuum (Steketee 1958; Maruyama 1964; Segall 2010). Different model structures have been assumed depending on the target phenomena: 2-D antiplane dislocations to model long (or vicinity of)

strike-slip faults (Savage and Burford 1973), 2-D inplane dislocations to model long dip-slip faults like subduction zones (Savage 1983), and 3-D dislocations for general finite faults (Okada 1992). Progress in analytical and numerical solutions has succeeded in explaining various earthquake processes (Smith and Sandwell 2004; Kyriakopoulos et al. 2013) and clarifying the effects of crustal structures such as surface topography and elastic properties (Masterlark 2003; Williams and Wallace 2015; Langer et al. 2019).

It has been known that antiplane deformation due to uniform slips on earthquake faults is not primarily controlled by the shape of fault surfaces but rather by the location of fault tips. Based on the analytical solutions, Segall (2010) noted that surface deformation is independent of the dip of the fault for infinitely long buried faults in the homogeneous half-space, suggesting difficulty in inferring the dip angle from surface

*Correspondence:
Tomohisa Okazaki
tomohisa.okazaki@riken.jp
[1] RIKEN Center for Advanced Intelligence Project, 2-2-2 Hikaridai, Seika, Kyoto 619-0237, Japan

observations. Based on the numerical modeling, Okazaki et al. (2022) extended it including internal deformation due to curved surface faults in a heterogeneous elastic medium with surface topography, implying the universality of this property. However, these were limited to individual observations and their implications were not fully explored.

In this study, we precisely state these findings as the general principle of fault geometry invariance in antiplane dislocations. This is verified in a simple and intuitive manner for curved earthquake faults, surface topographies, and underground structures. Furthermore, as a theoretical consequence of invariance, we introduce a field-valued function of the location of fault tips, which we call the dislocation potential. We show that the dislocation potential contains complete information on crustal deformation due to arbitrary fault slips with lower degrees of freedom than the commonly used Green's functions and slip response functions (Okada 1992; Pan 2019). Therefore, the use of the dislocation potential can advance the crustal deformation analysis of general antiplane dislocations.

We present an analytical example to illustrate fault geometry invariance in explicit forms. We also present a numerical example of physics-informed neural networks (PINNs), which can solve partial differential equations using deep learning without supervised data (Raissi et al. 2019; Karniadakis et al. 2021). PINNs serve as mesh-free numerical solvers that are applicable to complex geometries and exhibit promising performances in seismology (Smith et al. 2020; Rasht-Behesht et al. 2022; Ren et al. 2024), including fault slips (Okazaki et al. 2022; Fukushima et al. 2023). We discuss PINNs because their continuous representations are suitable for modeling with dislocation potentials (Table 1). PINN forward solvers can only address one specific problem and must be retrained if any condition is altered; heavy training costs hamper simulations at many conditions. Here, we use a PINN to solve the dislocation potential and leverage fault geometry invariance to obtain crustal deformation resulting from variable fault slips; rapid inferences enable simulations at many conditions. This combination makes use of the characteristics of theory (fault geometry invariance) and method (neural networks).

Table 1 Comparison of solution methods for crustal deformation

Method	Representation	Crustal structure
Analytical	Continuous	Limited
Physics-informed neural network	Continuous	General
Discretization methods	Discrete	General

The framework with the dislocation potential would be effective for uncertainty quantification and inversion analysis of unknown fault geometries. Because iterative forward calculations are required owing to the nonlinear dependence on fault shapes, analytical Green's functions available only for simple crustal structures have been used to avoid remeshing costs in discretization methods. Fault geometry invariance and the dislocation potential would enable these analyses for antiplane dislocations in realistic crustal structures.

2 Fault geometry invariance

We suppose antiplane dislocations in isotropic linear elastic media, where the crustal structure is uniform along one horizontal direction and the displacement field is parallel to it. The fault surfaces and their endpoints are termed dislocation surfaces and dislocation lines, respectively.

First, we formally state the principle of fault geometry invariance in antiplane dislocations. In a general underground structure with surface topography, uniform slips s on faults Σ_1 and Σ_2 with common dislocation lines produce displacement fields that are identical except for the constant difference s in a region D enclosed by Σ_1 and Σ_2 (Fig. 1a):

$$u_{\Sigma 2} = \begin{cases} u_{\Sigma 1} + s & \text{in} D \\ u_{\Sigma 1} & \text{elsewhere} \end{cases} \tag{1}$$

Here, Σ_1 and Σ_2 can be surface faults (Fig. 1a, top) or buried faults (Fig. 1a, bottom), as long as all the dislocations lines are common. This indicates that dislocation lines essentially determine crustal deformation, and that dislocation surfaces only change the position of the displacement discontinuity. This implies that the strain is independent of the dislocation surfaces and is thus continuous across them.

This statement can be deduced as follows: Suppose a combined fault slip ($\Sigma_2 - \Sigma_1$), where the minus sign represents a slip in the opposite direction (Fig. 1b). This corresponds to a boundary condition imposing displacement discontinuity s on Σ_1 and Σ_2 at the side toward D. Because s is constant throughout the boundary, its solution is given by a relative rigid motion s between D and the outer region without internal deformation:

$$u_{\Sigma 2 - \Sigma 1} = \begin{cases} s & \text{in} D \\ 0 & \text{elsewhere} \end{cases} \tag{2}$$

The linearity of deformation leads to Eq. (1). This derivation clarifies that fault geometry invariance holds only for a uniform slip in antiplane dislocations. For instance, in inplane problems, a uniform relative motion causes
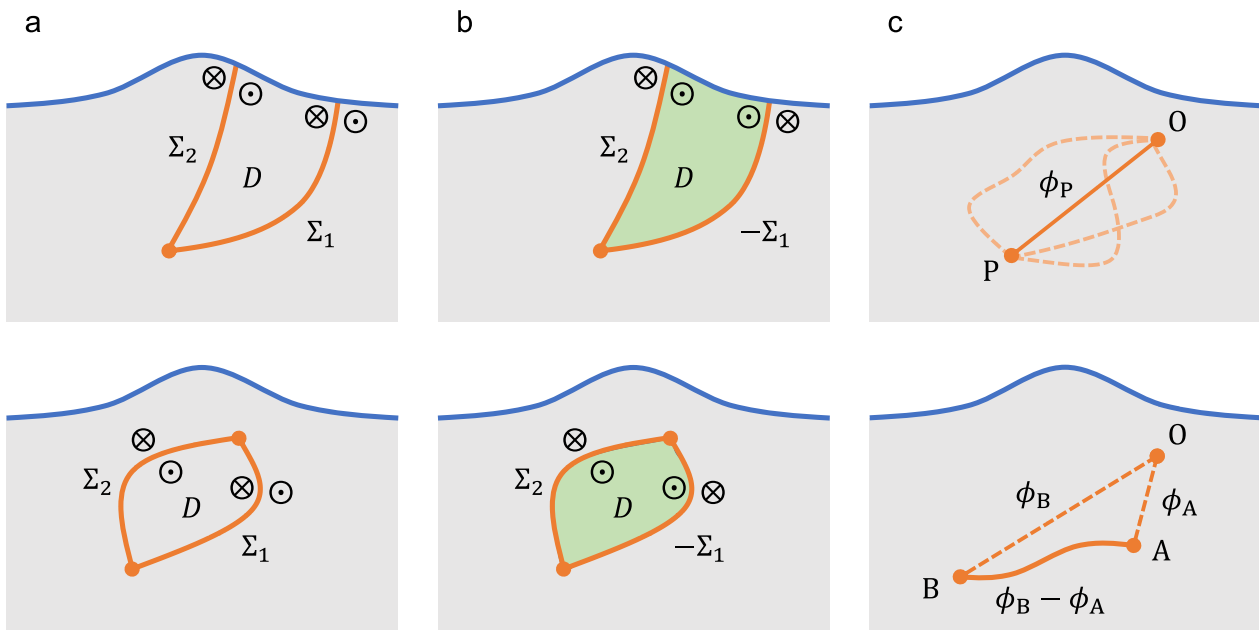
Fig. 1 Fault geometry invariance and dislocation potential. **a** Fault geometry invariance. Displacement fields due to uniform slips on two faults Σ_1 and Σ_2 with common dislocation lines are identical except for a constant difference in the region D enclosed by the two faults. The top and bottom panels illustrate surface and buried faults, respectively. Symbols ⊙ and ⊗ represent movements toward and away from the paper, respectively. **b** Derivation of the fault geometry invariance. The dislocation $(\Sigma_2 - \Sigma_1)$ yields a relative rigid motion between D and the outer region. **c** The dislocation potential. Top: For a fixed reference point O, the dislocation potential ϕ_P is defined as the displacement field due to the unit slip on linear faults connecting O and dislocation lines P. Bottom: Crustal deformation due to the unit slip on a general curved fault with dislocation lines A and B is given by the difference in ϕ between its endpoints.

deformation unless the boundary has a constant curvature (Fukahata and Matsu'ura 2016). See supplementary information Text S1 for a formal derivation based on the governing equations.

Fault geometry invariance unveils an intrinsic property of antiplane dislocations but does not have a direct implication for distributed slips. We now introduce a novel physical quantity, the dislocation potential, that leads to a streamlined crustal deformation analysis of distributed slips. The logic is analogous to the potential energy in classical mechanics (Goldstein et al. 2002): if the total work depends only on initial and final states but is independent of intermediate paths (i.e., conservative force), we can define a potential energy from which the work over arbitrary paths can be evaluated. The potential energy plays an essential role in various physical systems such as the gravitational and electrostatic forces.

Fault geometry invariance states that the displacement field depends only on dislocation lines (fault tips) but is independent of dislocation surfaces (intermediate shapes). Therefore, we can define a dislocation potential from which the displacement field caused by arbitrary fault shapes can be evaluated: by fixing a reference point O in the medium, the dislocation potential ϕ_P at a point P is defined by the displacement field due to the unit slip on a dislocation surface connecting the dislocation lines O and P. Because the displacement field is independent of intermediate shapes connecting O and P owing to the invariance, we choose a linear fault for clarity (Fig. 1c, top). We note that the gravitational and electrostatic potentials have a value on a scalar, whereas the dislocation potential has a value on a field. The displacement field due to the unit slip on a general fault Σ with dislocation lines A and B is represented by the difference in ϕ (Fig. 1c, bottom):

$$u_\Sigma = \phi_B - \phi_A \tag{3}$$

This formula can be extended to the distributed fault slips; by taking the arc-length parameter ξ on Σ, the displacement field due to a slip $s(\xi)$ is represented by a line integral of the directional differential of ϕ along Σ:

$$u_\Sigma = \int_\Sigma s(\xi)\nabla_\xi \phi_{P(\xi)} d\xi \tag{4}$$

Therefore, for a given crustal structure, the dislocation potential ϕ contains all information on crustal deformation. See supplementary information Text S2 for detailed discussion and derivations.

3 Analytical example

We presented a simple but abstract derivation of fault geometry invariance. Here, we illustrate it through explicit calculations. Internal deformation caused by a uniform slip b on a dipping fault in a homogeneous half-space is given by (Singh and Rani 1996)

$$u_1 = \frac{b}{2\pi}\left[\tan^{-1}\left(\frac{s - x_2\cos\delta - x_3\sin\delta}{x_3\cos\delta - x_2\sin\delta}\right) - \tan^{-1}\left(\frac{s - x_2\cos\delta + x_3\sin\delta}{x_3\cos\delta + x_2\sin\delta}\right)\right]_{s_1}^{s_2} \tag{5}$$

where δ is the dip angle, s is the radial coordinate, and x_2 and x_3 are the horizontal and vertical (downward positive) coordinates, respectively (Fig. 2). Fault geometry invariance indicates that Eq. (5) does not depend on δ (i.e., inclination of the dislocation surface) but depends only on the position of the dislocation lines. In fact, a straightforward calculation yields (supplementary information Text S3)

$$u_1 = \frac{b}{2\pi}\left[\left\{\tan^{-1}\left(\frac{x_3 - d_2}{x_2 - a_2}\right) - \tan^{-1}\left(\frac{x_3 + d_2}{x_2 - a_2}\right)\right\} - \left\{\tan^{-1}\left(\frac{x_3 - d_1}{x_2 - a_1}\right) - \tan^{-1}\left(\frac{x_3 + d_1}{x_2 - a_1}\right)\right\}\right] \tag{6}$$

This coincides with deformation due to two vertical faults (Fig. 2a): the first and second terms represent deformation fields due to dislocation and image sources with slip b at (a_2, d_2), respectively, whereas the third and fourth terms represent those due to dislocation and image source with slip $-b$ at (a_1, d_1), respectively (Segall 2010). This reduction suggests that the derivation of analytical solutions can be considerably simplified by appropriately considering fault geometry invariance. Although we treated a linear fault for explicit calculations, fault geometry invariance ensures that Eq. (6) holds for curved faults.

4 Physics-informed learning application

We now demonstrate the utility of ϕ through a numerical example using PINNs, whose mesh-free property is suitable for modeling ϕ. As previously mentioned, PINN forward modeling addresses one specific problem and must be retrained when some of the parameters are altered, which incurs additional computational costs. In general, this limitation can be resolved by adding parameters that specify model structures to the input variables. This is called surrogate modeling and straightforward for finite-dimensional quantities such as strength and position (Sun et al. 2020; Song and Wang 2023). However, adding infinite-dimensional quantities such as functions and shapes requires representations in parametric forms (Ren et al. 2024; Sun et al. 2020), which incurs a trade-off between the expressive power and the training tractability.

Based on fault geometry invariance, we can construct a PINN surrogate model for crustal deformation due to infinite-dimensional fault geometry (curve) and slip distribution (function) without finite-dimensional parametric forms. The PINN approximates the dislocation potential $\phi_{(X, Y)}(x, y)$, which represents the
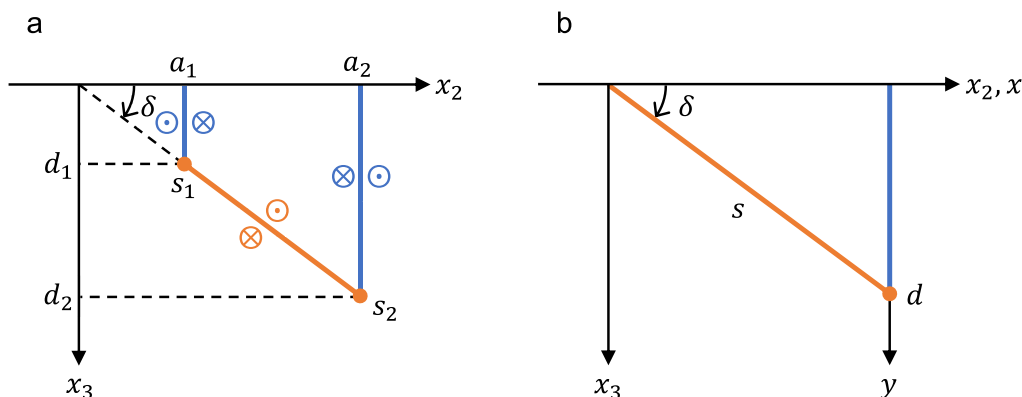

Fig. 2 Fault geometry invariance for linear faults in a homogeneous half-space. **a** Internal deformation due to a uniform slip on a dipping fault (orange line) is identical to that on two vertical faults (blue lines) owing to fault geometry invariance. **b** Coordinate transformation that relates the dipping and vertical faults

displacement at (x, y) due to a unit slip on a fault connecting a reference point O and (X, Y). The input variables are (x, y, X, Y) and the output variable is ϕ. Because of the singularity at dislocation lines, care must be taken to approximate ϕ using neural networks. We fix a reference point O at the ground surface to avoid singularity at O. To remove the singularity at the dislocation line (X, Y), we introduce a polar coordinate system whose pole and branch cut coincide with the dislocation line and surface, respectively (Fig. 3a). Because infinite fault planes with variable dislocation lines are solved simultaneously, the pole location varies with the input variables. We define a fixed coordinate transformation $T : (x, y, X, Y) \rightarrow (r, \theta, X, Y)$ by

$$r = \sqrt{(x - X)^2 + (y - Y)^2}, \theta = \tan^{-1}\left(\frac{x - X}{y - Y}\right) \tag{7}$$

We then construct a neural network $f_{NN} : (r, \theta, X, Y) \rightarrow \phi$, which is regular in the whole input domain. Consequently, the dislocation potential can be expressed as a composite function (Fig. 3b):

$$\phi_{(X, Y)}(x, y) = (f_{NN} \circ T)(x, y, X, Y) \tag{8}$$

The loss function is the same as that of the forward modeling (Okazaki et al. 2022). By simply adding the 2-D position (X, Y) of dislocation lines to the input variables of the PINN forward model (Okazaki et al. 2022), the resultant PINN can solve the dislocation potential $\phi_{(X, Y)}(x, y)$ and can be used to estimate crustal deformation resulting from arbitrary fault slips using Eq. (4).

In essence, fault geometry invariance reduces the infinite-dimensional space of curves and functions to the 2-D space of positions. See supplementary information Text S4 for the implementation of PINNs.

Figure 4 shows the results in a homogeneous half-space (examples of the learned dislocation potentials are shown in Fig. S1), which are in good agreement with analytical solutions (Singh and Rani 1996); the errors are shown in Fig. S2. Figure 5 shows the results in a heterogeneous medium with a surface topography for which analytical solutions are unavailable (examples of the learned dislocation potentials are shown in Fig. S3). PINNs can represent continuous geometric shapes and changes in elastic properties without discretization. Supposing that a fault slip reaches the surface, but its distribution in depth is uncertain, we present the estimations for different fault slips. The estimated surface displacements for variable faults are shown in Fig. 5c (faults in Fig. 5a with the coolest color slip in Fig. 5b) and variable slips in Fig. 5d (white fault in Fig. 5a with slip distributions in Fig. 5b). Although only five models are plotted in each panel for visibility, hundreds or thousands of estimations can be performed in a reasonable time owing to the rapid forward computation of neural networks. Additional calculations of the combination of different fault shapes and slip amounts would clarify their relationship and trade-off. If we solve deformation separately, computational time will range 10 min−5 h for each fault slip (Okazaki et al. 2022). By modeling the dislocation potential, it reduces to −0.4 s for each fault slip. The PINN solver shows full potential for calculating the deformation fields resulting from many possible rupture scenarios.
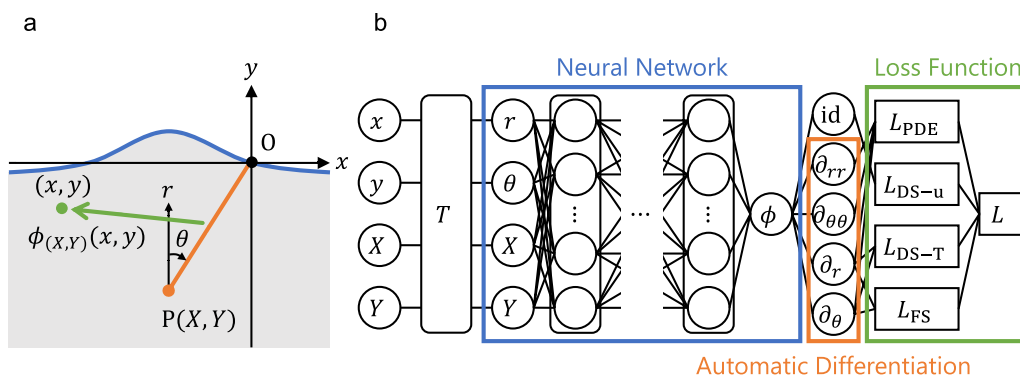

Fig. 3 Physics-informed neural networks (PINNs) for dislocation potential modeling. **a** The coordinate system for the modeling. The reference point O of the dislocation potential is set at the ground surface. The Cartesian coordinates (X, Y) and (x, y) denote the dislocation line P and the evaluation point of the displacement field, respectively. The polar coordinates (r, θ) are introduced so that the pole coincides with the dislocation line. **b** The PINN structure. The input variables (x, y, X, Y) are transformed to (r, θ, X, Y) and a neural network converts it to the dislocation potential $\phi_{(X, Y)}(x, y)$. The loss function is identical to that in the forward modeling (see supplementary information Text S4 for the individual terms)
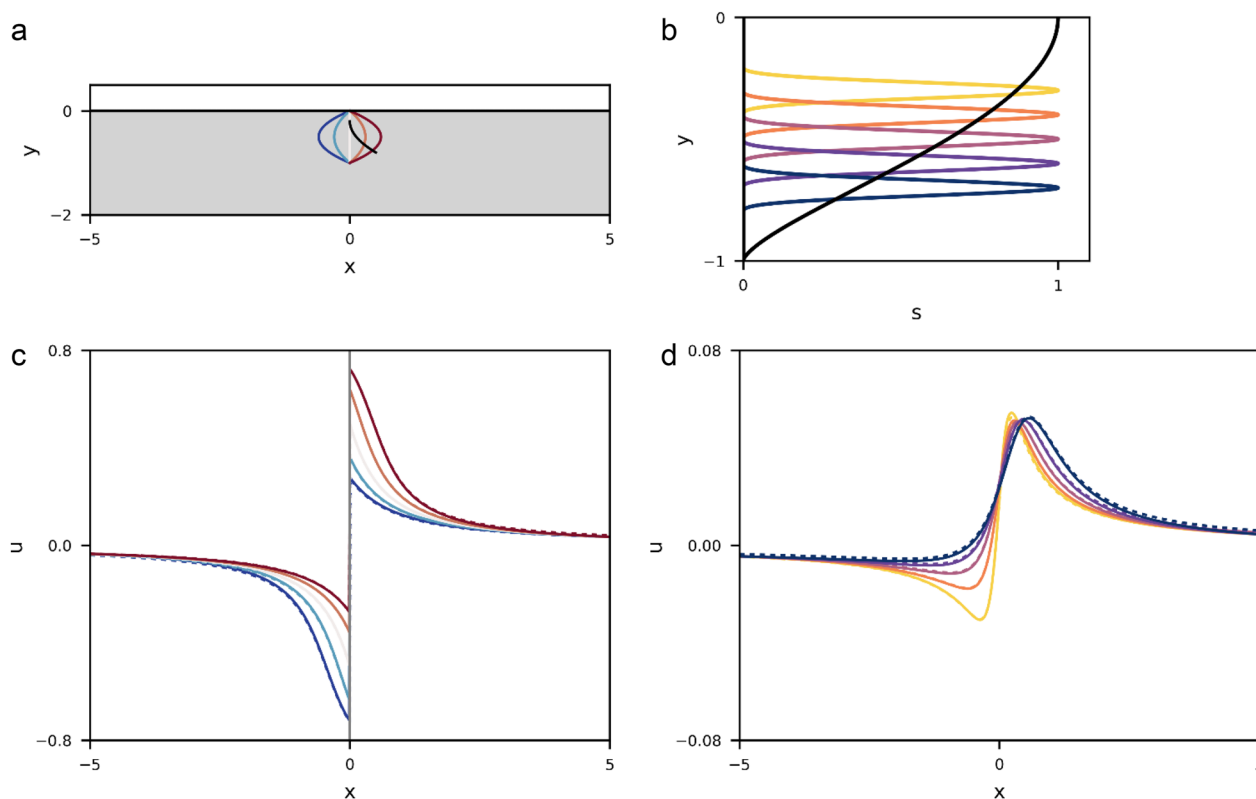
Fig. 4 Physics-informed modeling results in the homogeneous half-space. **a** Fault geometries. **b** Slip distributions on the faults. **c** Surface displacements due to a tapered slip (black line in b). Colors represent the fault geometries in **a**. The vertical line indicates the fault location at the ground surface. **d** Surface displacements due to a buried fault (black line in a). Colors represent slip distributions in **b**. In **c** and **d**, Solid and dashed lines indicate physics-informed neural network and analytical solutions, respectively

5 Discussion

We introduced the dislocation potential as a consequence of fault geometry invariance. Green's function, the displacement field due to a point force, is the most general element of crustal deformation, including explosive and shear sources. Its analytical expressions enable rapid calculations of deformation due to arbitrary finite sources, but are limited to relatively simple structures, such as homogeneous/layered flat/spherical media (Okada 1992; Pollitz 1996; Nikkhoo and Walter 2015). For complex structures, numerical methods have difficulty in treating point forces for Green's functions, and thus calculate the slip response function, the displacement field due to a dislocation source (Ohtani and Hirahara 2015; Hori et al. 2021). The set of dislocation potentials constitutes a subset of that of slip response functions; the latter is an infinite-dimensional space consisting of arbitrary dislocation surfaces (curves in a 2-D space), whereas the former is a 2-D space consisting of linear faults connecting a reference point and arbitrary dislocation lines (points in a 2-D space). Notably, the dislocation potential possesses

the same information of crustal deformation as the slip response function owing to fault geometry invariance.

We presented analytical and PINN examples, because they represent solutions as continuous functions (Table 1). This property is suitable for modeling the dislocation potential, whose derivatives are used for subsequent calculations. In contrast, conventional numerical solvers represent solutions at discrete grids or meshes, which complicates the direct use of the dislocation potential. Nevertheless, the theory also applies to these methods and can be useful by using appropriate interpolations.

There is a limitation that fault geometry invariance holds in antiplane dislocations but cannot be generalized to inplane and 3-D dislocations, as understood from the derivation. The principle of superposition holds for linear elastic and viscoelastic materials, but not for nonlinear rheology. The possibility of simultaneous solutions is summarized in Table 2. This shows how theoretical insights can improve the efficiency of modeling of specific problems.
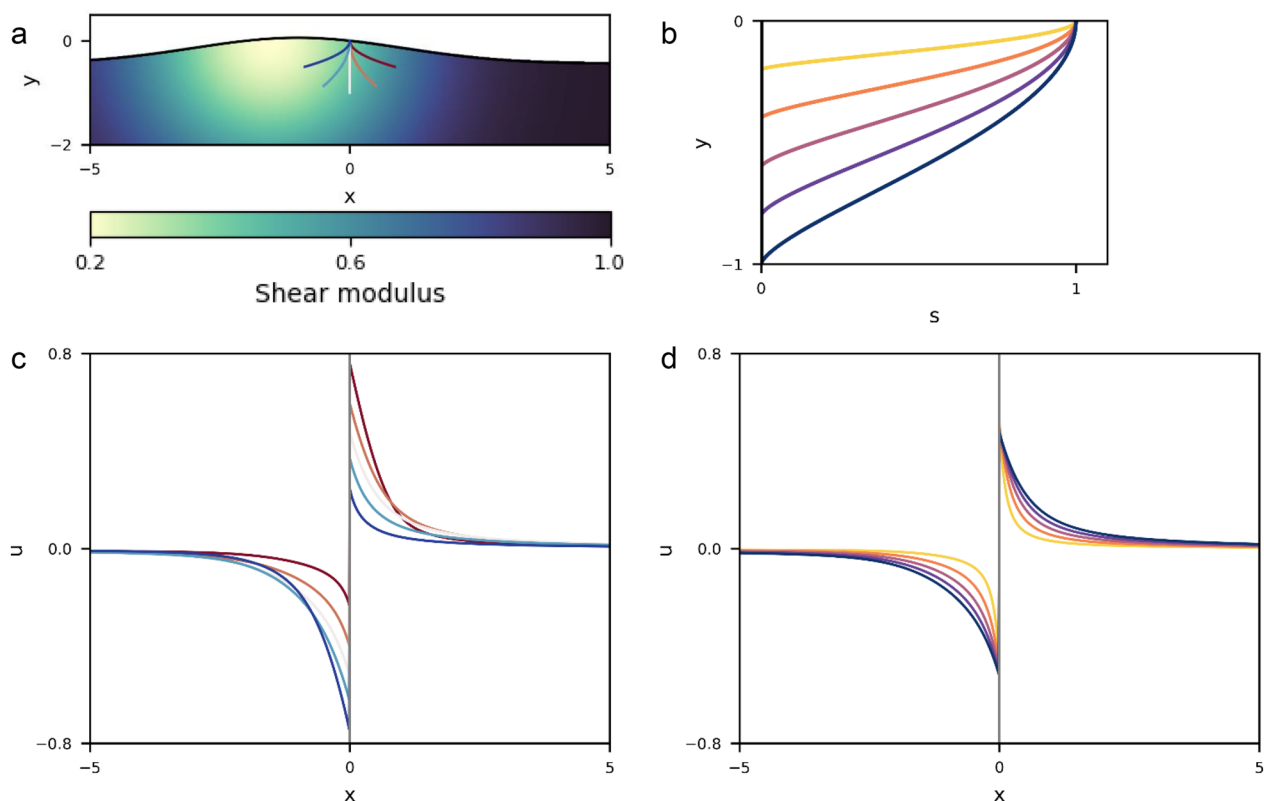
Fig. 5 Physics-informed modeling results in the heterogeneous structure. **a** Crustal structure and fault geometries. **b** Slip distributions on the faults. **c** Surface displacement due to a tapered slip (the coolest color line in **b**). Colors represent the fault geometries in **a**. **d** Surface displacement due to a vertical fault (white line in **a**). Colors represent slip distributions in **b**. In **c** and **d**, vertical lines indicate the fault location at the ground surface

Table 2 Possibility of simultaneous solutions for crustal deformation

Problem	Topography	Elastic property	Fault geometry	Slip distribution
General	Fixed	Fixed	Fixed	Fixed
Linear material	Fixed	Fixed	Fixed	Simultaneous
Linear antiplane	Fixed	Fixed	Simultaneous	Simultaneous

Fault geometry invariance elucidates a fundamental nature of antiplane crustal deformation with a clear derivation. Its theoretical consequence, the dislocation potential, enables a streamlined analysis with straightforward extensions of existing methods, as exemplified by the PINN modeling. The dislocation potential can be used to quantify the uncertainty of surface deformation resulting from the limited knowledge of fault ruptures in depth. Another promising application is inversion analysis of earthquake source processes, especially the simultaneous estimation of fault geometry and slip distribution. Owing to the nonlinear dependence on fault shapes, analytical Green's functions in simple structures have been used to perform iterative estimations (Ragon et al. 2018; Dutta et al. 2021; Shimizu et al. 2021). The presented PINN model can be incorporated as a forward subroutine into sampling-based inversion analyses in complex structures, and may be developed to directly perform inverse modeling (Rasht-Behesht et al. 2022; Chen et al. 2022; Agata et al. 2023). Modeling with the dislocation potential in other solution methods can also be explored. Fault geometry invariance and dislocation potential would broaden the scope of antiplane deformation analysis involving uncertain fault slips in complex crustal structures.

Scientific machine learning (SciML) is a new research trend that uses deep learning techniques for modeling physical systems, including those in solid and fluid

Okazaki *et al. Progress in Earth and Planetary Science*   (2024) 11:52

Page 8 of 9

Table 3 Comparison of scientific machine learning methods

Modeling task	Forward modeling	Surrogate modeling	Operator learning[*]
Input condition	Fixed	Finite dimension	Infinite dimension[*]
Method	PINN	PINN[*]	Neural operator
Representation	Continuous	Continuous[*]	Discrete
Input variable	Spacetime variable	Spacetime variable and input condition[*]	Input condition (discretized)
Output variable	Solution	Solution[*]	Solution (discretized)
Training cost	Low	Medium[*]	High

The superscript [*] indicates this study. PINN, physics-informed neural network

Earth sciences (Baker et al. 2019). PINNs are representative methods capable of forward and finite-dimensional surrogate modeling with continuous representations (Sect. 4). Moreover, some physical conditions, such as initial states and spatial variations of material properties, have infinite dimensions. To learn operators between infinite-dimensional spaces, neural operators have been investigated (Lu et al. 2021; Kovachki et al. 2023) and applied to various scientific tasks such as numerical weather forecasts (Pathak et al. 2022) and seismic wave simulations (Yang et al. 2021). However, training costs and model complexity with discrete representations are limitations of neural operators (Table 3). In this study, we constructed a PINN surrogate model of the dislocation potential and leveraged fault geometry invariance to calculate crustal deformation for infinite-dimensional fault slip conditions. In other words, an operator learning problem (the right column in Table 3) was solved with PINNs (the middle column in Table 3) owing to a theory. This construction illustrates how a theoretical insight into target phenomena can sophisticate geophysical modeling with SciML approaches.

Abbreviations
PINN   Physics-informed neural network
SciML   Scientific machine learning

Supplementary Information
The online version contains supplementary material available at https://doi.org/10.1186/s40645-024-00654-7.

Additional file 1.

References
Agata R, Shiraishi K, Fujie G (2023) Bayesian seismic tomography based on velocity-space stein variation gradient descent for physics-informed neural network. IEEE Trans Geosci Remote Sens 61:1–17. https://doi.org/10.1109/TGRS.2023.3295414

Baker N, Alexander F, Bremer T et al (2019) Workshop report on basic research needs for scientific machine learning: core technologies for artificial intelligence. USDOE Office of Science (SC), Washington, DC. https://doi.org/10.2172/1478744

Chen Y, de Ridder SA, Rost S, Guo Z, Wu X, Chen Y (2022) Eikonal tomography with physics-informed neural networks: rayleigh wave phase velocity in the northeastern margin of the Tibetan plateau. Geophys Res Lett 49(21):e2022GL099053. https://doi.org/10.1029/2022GL099053

Dutta R, Jónsson S, Vasyura-Bathke H (2021) Simultaneous Bayesian estimation of non-planar fault geometry and spatially-variable slip. J Geophys Res Solid Earth 126:e2020JB020441. https://doi.org/10.1029/2020JB020441

Freed A, Bürgmann R (2004) Evidence of power-law flow in the Mojave Desert mantle. Nature 430:548–551. https://doi.org/10.1038/nature02784

Fukahata Y, Matsu'ura M (2016) Deformation of island-arc lithosphere due to steady plate subduction. Geophys J Int 204(2):825–840. https://doi.org/10.1093/gji/ggv482

Fukushima R, Kano M, Hirahara K (2023) Physics-informed neural networks for fault slip monitoring: simulation, frictional parameter estimation, and prediction on slow slip events in a spring-slider system. J Geophys Res Solid Earth 128(12):e2023JB027384. https://doi.org/10.1029/2023JB027384

Goldstein H, Poole C, Safko J (2002) Classical mechanics. Addison Wesley, Boston

Hori T, Agata R, Ichimura T, Fujita K, Yamaguchi T, Iinuma T (2021) High-fidelity elastic green's functions for subduction zone models consistent with the global standard geodetic reference system. Earth Planets Space 73(1):41. https://doi.org/10.1186/s40623-021-01370-y

Karniadakis GE, Kevrekidis IG, Lu L, Perdikaris P, Wang S, Yang L (2021) Physics-informed machine learning. Nat Rev Phys 3:422–440. https://doi.org/10.1038/s42254-021-00314-5

Kovachki N, Li Z, Liu B, Azizzadenesheli K, Bhattacharya K, Stuart A, Anandkumar A (2023) Neural operator: learning maps between function spaces with applications to PDEs. J Mach Learn Res 24:1–97

Kyriakopoulos C, Masterlark T, Stramondo S, Chini M, Bignami C (2013) Coseismic slip distribution for the Mw 9 2011 Tohoku-Oki earthquake derived

Okazaki *et al. Progress in Earth and Planetary Science*   (2024) 11:52

Page 9 of 9

from 3-D FE modeling. J Geophys Res Solid Earth 118:3837–3847. https://doi.org/10.1002/jgrb.50265

Langer L, Gharti HN, Tromp J (2019) Impact of topography and three-dimensional heterogeneity on coseismic deformation. Geophys J Int 217(2):866–878. https://doi.org/10.1093/gji/ggz060

Lu L, Jin P, Pang G, Zhang Z, Karniadakis GE (2021) Learning nonlinear operators via DeepONet based on the universal approximation theorem of operators. Nat Mach Intell 3:218–229. https://doi.org/10.1038/s42256-021-00302-5

Maruyama T (1964) Statical elastic dislocation in an infinite and semi-infinite medium. Bull Earthq Res Inst 42:289–368

Masterlark T (2003) Finite element model predictions of static deformation from dislocation sources in a subduction zone: sensitivities to homogeneous, isotropic, Poisson-solid, and half-space assumptions. J Geophys Res 108:2540. https://doi.org/10.1029/2002JB002296

Nikkhoo M, Walter TR (2015) Triangular dislocation: an analytical, artefact-free solution. Geophys J Int 201(2):1119–1141. https://doi.org/10.1093/gji/ggv035

Ohtani M, Hirahara K (2015) Effect of the Earth's surface topography on quasi-dynamic earthquake cycles. Geophys J Int 203(1):384–398. https://doi.org/10.1093/gji/ggv187

Okada Y (1992) Internal deformation due to shear and tensile faults in a half-space. Bull Seismol Soc Am 82(2):1018–1040. https://doi.org/10.1785/BSSA0820021018

Okazaki T, Ito T, Hirahara K, Ueda N (2022) Physics-informed deep learning approach for modeling crustal deformation. Nat Commun 13:7092. https://doi.org/10.1038/s41467-022-34922-1

Pan E (2019) Green's functions for geophysics: a review. Rep Prog Phys 82(10):106801. https://doi.org/10.1088/1361-6633/ab1877

Pathak J, Subramanian S, Harrington P et al (2022) FourCastNet: a global data-driven high-resolution weather model using adaptive Fourier neural operators. Preprint at https://doi.org/10.48550/arXiv.2202.11214

Pollitz FF (1996) Coseismic deformation from earthquake faulting on a layered spherical earth. Geophys J Int 125(1):1–14. https://doi.org/10.1111/j.1365-246X.1996.tb06530.x

Pollitz FF, Wicks C, Thatcher W (2001) Mantle flow beneath a continental strike-slip fault: postseismic deformation after the 1999 hector mine earthquake. Science 293(5536):1814–1818. https://doi.org/10.1126/science.1061361

Ragon T, Sladen A, Simons M (2018) Accounting for uncertain fault geometry in earthquake source inversions–I. Theory and simplified application. Geophys J Int 214:1174–1190. https://doi.org/10.1093/gji/ggy187

Raissi M, Perdikaris P, Karniadakis GE (2019) Physics-informed neural networks: a deep learning framework for solving forward and inverse problems involving nonlinear partial differential equations. J Comput Phys 378:686–707. https://doi.org/10.1016/j.jcp.2018.10.045

Rasht-Behesht M, Huber C, Shukla K, Karniadakis GE (2022) Physics-informed neural networks (PINNs) for wave propagation and full waveform inversions. J Geophys Res Solid Earth 127:e2021JB023120. https://doi.org/10.1029/2021JB023120

Ren P, Rao C, Chen S, Wang J-X, Sun H, Liu Y (2024) SeismicNet: physics-informed neural networks for seismic wave modeling in semi-infinite domain. Comput Phys Commun 295:109010. https://doi.org/10.1016/j.cpc.2023.109010

Savage JC (1983) A dislocation model of strain accumulation and release at a subduction zone. J Geophys Res 88(B6):4984–4996. https://doi.org/10.1029/JB088iB06p04984

Savage JC, Burford RO (1973) Geodetic determination of relative plate motion in central California. J Geophys Res 78(5):832–845. https://doi.org/10.1029/JB078i005p00832

Segall P (2010) Earthquake and volcano deformation. Princeton University Press, Princeton

Shimizu K, Yagi Y, Okuwaki R, Fukahata Y (2021) Construction of fault geometry by finite-fault inversion of teleseismic data. Geophys J Int 224:1003–1014. https://doi.org/10.1093/gji/ggaa501

Singh SJ, Rani S (1996) 2-D modelling of crustal deformation associated with strike-slip and dip-slip faulting in the Earth. Proc Natl Acad Sci India Sect A 66:187–215

Smith B, Sandwell D (2004) A three-dimensional semianalytic viscoelastic model for time-dependent analyses of the earthquake cycle. J Geophys Res 109:B12401. https://doi.org/10.1029/2004JB003185

Smith JD, Azizzadenesheli K, Ross ZE (2020) EikoNet: solving the Eikonal equation with deep neural networks. IEEE Trans Geosci Remote Sens 59(12):10685–10696. https://doi.org/10.1109/TGRS.2020.3039165

Song C, Wang Y (2023) Simulating seismic multifrequency wavefields with the Fourier feature physics-informed neural network. Geophys J Int 232:1503–1514. https://doi.org/10.1093/gji/ggac399

Steketee JA (1958) Some geophysical applications of the elasticity theory of dislocations. Can J Phys 36(9):1168–1198. https://doi.org/10.1139/p58-123

Sun T, Wang K, Iinuma T, Hino R, He J, Fujimoto H, Kido M, Osada Y, Miura S, Ohta Y, Hu Y (2014) Prevalence of viscoelastic relaxation after the 2011 Tohoku-oki earthquake. Nature 514:84–87. https://doi.org/10.1038/nature13778

Sun L, Gao H, Pan S, Wang J-X (2020) Surrogate modeling for fluid flows based on physics-constrained deep learning without simulation data. Comput Methods Appl Mech Eng 361:112732. https://doi.org/10.1016/j.cma.2019.112732

Williams CA, Wallace LM (2015) Effects of material property variations on slip estimates for subduction interface slow-slip events. Geophys Res Lett 42(4):1113–1121. https://doi.org/10.1002/2014GL062505

Yang Y, Gao AF, Castellanos JC, Ross ZE, Azizzadenesheli K, Clayton RW (2021) Seismic wave propagation and inversion with neural operators. Seism Rec 1(3):126–134. https://doi.org/10.1785/0320210026

Publisher's Note